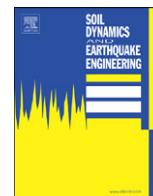




ELSEVIER

Contents lists available at ScienceDirect

Soil Dynamics and Earthquake Engineering

journal homepage: www.elsevier.com/locate/soildyn

Development of the ElarmS methodology for earthquake early warning: Realtime application in California and offline testing in Japan

Holly M. Brown*, Richard M. Allen, Margaret Hellweg, Oleg Khainovski, Douglas Neuhauser, Adeline Souf

Seismological Laboratory, University of California, Berkeley, CA, USA

ARTICLE INFO

Article history:

Received 27 October 2009

Received in revised form

15 March 2010

Accepted 16 March 2010

Keywords:

Earthquake early warning

CISN

Realtime

California

Japan

ElarmS

ABSTRACT

In July 2009, the California Integrated Seismic Network concluded a three-year study of earthquake early warning systems in California. Three algorithms were expanded and examined during the study. Here we discuss the history, methodology, and performance of one of the algorithms, ElarmS. Earthquake Alarm Systems, or ElarmS, uses peak displacement and maximum predominant frequency of the P-wave to detect earthquakes and quantify their hazard in the seconds after rupture begins. ElarmS was developed for Northern and Southern California, and now processes waveforms in realtime from 603 seismic sensors across the state. We outline the methodology as currently implemented, present several example events from different regions of California, and summarize the performance in terms of false and missed alarms. ElarmS was also tested offline with a dataset of 84 large magnitude earthquakes from Japan. The results from the Japan dataset were used to create a statistical error model for the algorithm. The model can be used to provide realtime uncertainty estimates at any stage in processing. In August 2009 the CISN embarked on a second three-year study of earthquake early warning. As part of this ongoing research, we identify the technological and methodological challenges facing ElarmS. Telemetry latencies and false alarm rates are two key opportunities for improvement.

© 2010 Elsevier Ltd. All rights reserved.

1. Introduction

Earthquake early warning (EEW) systems are algorithms that detect the initial P-waves from an earthquake, rapidly estimate the location and magnitude of the event, and then predict subsequent ground shaking in the surrounding region. EEW systems offer the potential for a few seconds to a few tens of seconds warning prior to hazardous ground shaking: enough time for individuals to get to a safe location, perhaps under a sturdy table, for shutdown of utilities, slowing of trains, and other automated steps to reduce hazards from ground shaking.

In July 2009, the California Integrated Seismic Network (CISN) completed a three-year investigation into the viability of an EEW system in California. Three algorithms were expanded, tested, and compared during the study: Onsite, a single-station method that uses τ_c and P_d [8], Virtual Seismologist, a network-based method that uses peak amplitudes and Bayesian statistics [10], and ElarmS, a network-based method that uses τ_p^{\max} and $P_{d/v}$ [5].

* Corresponding author. Tel.: 510 642 6994. Fax: 510 643 5811.
E-mail address: hollybrown@berkeley.edu (H.M. Brown).

The goal of the three-year project was to determine whether EEW is feasible in California. Results from each algorithm were continuously reported to a central database run by the Southern California Earthquake Center (SCEC) for analysis. By the end of the three years, all three algorithms had successfully predicted ground shaking before it was felt for many earthquakes in the state. At the end of the study the CISN determined that EEW is feasible, potentially desirable, and within reach for California. In August 2009 a second three-year study was initiated, to integrate the three test algorithms into a single prototype EEW system and provide realtime warning to a small group of test users by the end of the study in summer 2012.

Here we delineate the methodology, progress, and results of the ElarmS algorithm, which is now an integral part of the forthcoming prototype CISN EEW system. The ElarmS algorithms for magnitude and location estimation were developed offline with two datasets of events from Northern and Southern California. Those algorithms are now used in realtime, continuously processing waveforms from throughout the state of California and producing predictions of ground shaking within seconds of event detection. A separate dataset of events from Japan was processed offline to test ElarmS' performance for large events. From the Japan results we developed an error model which can be used in realtime to estimate the uncertainty in any ElarmS prediction.

2. Development and methodology

2.1. Overview

Earthquake Alarm Systems, or ElarmS, is a network-based EEW system. The algorithm detects P-wave arrivals at several stations around an event epicenter and uses the amplitude and frequency content of the P-wave to rapidly estimate the magnitude and hypocenter of the event. Estimates from several stations are combined to improve accuracy and minimize the chance of a false alarm. ElarmS then applies the estimated magnitude and location to CISM ShakeMap regional ground motion prediction equations (GMPEs) to produce a realtime prediction of impending ground shaking. Predictions above a certain threshold prompt an automatic alert message that can be sent to users.

The ElarmS algorithm is divided into a waveform processing module and an event monitoring module. The waveform processing module analyzes raw waveforms from all contributing stations, detects P-wave arrivals, and calculates the necessary ElarmS parameters: predominant period, peak amplitudes, signal-to-noise ratio (SNR), peak ground acceleration and velocity (PGA and PGV), and trigger times. These parameters are then passed to the event monitor, which associates the triggers into an event, estimates the event location, estimates the magnitude, and predicts ground shaking. As additional stations record P-wave arrivals, the waveform processing module passes their parameters to the event monitor, which includes them into the event analysis [3,5].

2.2. Location

Event location is estimated by a four-stage algorithm, defined by the number of station triggers. When a single station triggers, the event is located directly beneath the station, at a depth of 8 km. When two stations have triggered, the event is located between them based on arrival times, again at a depth of 8 km. When three stations have triggered, ElarmS uses a two-dimensional grid search at a depth of 8 km to determine the hypocenter and origin time that minimize arrival time residuals. Finally, once four or more stations have triggered, ElarmS performs a three-dimensional grid search, with depth intervals every 10 km, to estimate the hypocenter and origin time that minimizes arrival time residuals. In California, most events occur at depths of 5–15 km and the average depth is 8 km [11]. Rather than determining depth, ElarmS sets the depth of all California earthquakes to 8 km. When processing events in Japan, all four stages are used including the depth determination.

2.3. Magnitude

ElarmS was originally developed from an empirically observed relationship between maximum predominant period, τ_p^{\max} , and final event magnitude [1,4,13,14]. For any vertical channel (broadband HHZ, or strong motion HLZ, HNZ), the predominant period time series is defined recursively by:

$$\tau_{p,i} = 2\pi(X_i/D_i)^{1/2}$$

where $X = \alpha X_{i-1} + x_i^2$ and $D_i = \alpha D_{i-1} + (d_x/d_t)i^2$. The constant α is a smoothing factor equal to $1-dt$, where dt is the sample interval, and x_i is the ground velocity of the last sample. Acceleration waveforms are integrated to velocity first, and all waveforms are filtered with a causal 2-pole, 3-Hz, low-pass Butterworth filter. τ_p^{\max} is then the maximum observed τ_p value during the first four seconds of P-wave arrival.

To determine the empirical scaling relations, all τ_p^{\max} values for a given region are plotted against the final magnitude of each event. A least squares fit to the data produces the scaling relation, which is then used in realtime to estimate magnitude (see Section 3.1).

In 2007 ElarmS was updated to utilize a second P-wave parameter, the peak amplitude [18]. As before, vertical-component waveforms are filtered with a 3 Hz low-pass Butterworth filter. Peak amplitudes observed during the first four seconds of P-wave arrival are scaled to an epicentral distance of 10 km and compared to the final catalog magnitude for the event. A least squares fit to the data provides a scaling relation for the region. Note that the peak amplitude scaling relations are dependent on the epicentral distance of the amplitude observation. In Northern California, peak displacement is used for broadband (HH) instruments and peak velocity is used for strong motion (HL and HN) instruments. Peak displacement has a theoretically longer period signal and thus less high frequency noise than peak velocity, but numerically integrating the acceleration signal twice (from acceleration to velocity, and again from velocity to displacement) introduces errors. We found that for acceleration instruments in Northern California, peak velocity provides a more robust scaling relation than does peak displacement. In Southern California and Japan, peak displacement produced the strongest scaling relation for all instruments, despite the double integration from acceleration. In general, we refer to the peak amplitude scaling relations as $P_{d/v}$ with the understanding that we may use P_d or P_v for any given site.

Although the scaling relations for τ_p^{\max} and $P_{d/v}$ are determined using four seconds of P-wave arrival, waiting for a full four seconds of P-wave to be available during realtime processing wastes valuable seconds of potential warning time. Instead ElarmS begins to apply the scaling relations and estimate magnitude as soon as a single station has observed a single full second of P-wave arrival (the first half-second is discarded). As additional seconds of P-wave become available, ElarmS recalculates τ_p^{\max} and $P_{d/v}$ accordingly. Since both τ_p^{\max} and $P_{d/v}$ are the maximum or peak values, they can only increase with additional seconds of data. The initial one-second magnitude estimate is therefore always a minimum estimate.

To ensure that early arriving S-waves at near-field stations do not interfere with the magnitude estimate which is P-wave based, ElarmS also utilizes a simple P/S filter, based on an S–P moveout of 8 km/s (with a minimum S–P time of 1 s, assuming most events are 8 km deep). The S–P time is estimated at each station given the event location and the P-waveform is only used up to the S-wave arrival. One potential drawback of this filter is that location errors may cause valid P-wave data to be discarded as misidentified S-waves.

For each triggering station, τ_p^{\max} and $P_{d/v}$ are scaled separately to create two independent estimates of magnitude. The estimates are then averaged to form a single event magnitude for that station. As additional stations report P-wave triggers, their magnitude estimates are averaged into the event magnitude, to provide an increasingly accurate description of the event as time passes.

2.4. Ground motions

Once location and magnitude have been estimated for an event, ground motion is predicted at each triggered station by applying the location and magnitude to CISM-defined ShakeMap GMPEs for the region [16]. The resulting “AlertMap” displays predicted ground shaking in the familiar ShakeMap format, i.e. a map of predicted shaking intensity. As peak ground shaking is

observed at individual stations, the observations are integrated into the shaking intensity map. ElarmS incorporates a bias correction by scaling the GMPE up or down to best-fit the available observations. Eventually, when all stations have reported peak ground shaking, the AlertMap looks much the same as the post-event ShakeMap.

The ElarmS algorithm has been tested with datasets from Northern California, Southern California, and Japan [2–5,9,13–15,18]. Each test dataset provided regional scaling relations for τ_p^{\max} and $P_{d/v}$, and utilized GMPEs specific to that location. Most recently ElarmS has been adapted to run in realtime throughout the state of California.

3. Application of ElarmS to California

3.1. Scaling and GMPEs

Offline tests of California earthquake datasets have produced separate scaling relations for Northern and Southern California events [15,18]. The magnitude scaling relations are determined empirically by comparing observed τ_p^{\max} and $P_{d/v}$ values to final catalog magnitude for a dataset of test events, with as wide a range of magnitudes as possible. Once determined, the scaling relations are used in realtime to estimate event magnitude, based on realtime observations of P-wave frequency and amplitude.

For northern California, Wurman et al. [18] analyzed a dataset of 43 events recorded by Berkeley Digital Seismic Network (BK)

and Northern California Seismic Network (NC) seismometers (Fig. 1) between 2001 and 2007, with magnitudes ranging from 3.0 to 7.1. The analysis resulted in the following scaling relations:

$$\begin{aligned} M_w &= 5.22 + 6.66 * \log_{10}(\tau_p^{\max}) && \text{for } \tau_p^{\max} \text{ on HHZ, HLZ, HNZ channels} \\ M_w &= 1.04 * \log_{10}(P_d) + 1.27 * \log_{10}(R) + 5.16 && \text{for } P_d \text{ on HH channels} \\ M_w &= 1.37 * \log_{10}(P_v) + 1.57 * \log_{10}(R) + 4.25 && \text{for } P_v \text{ on HL channels} \\ M_w &= 1.63 * \log_{10}(P_v) + 1.65 * \log_{10}(R) + 4.40 && \text{for } P_v \text{ on HN channels} \end{aligned}$$

where R is the epicentral distance to the station. The τ_p^{\max} and P_d relations are shown in Fig. 2a, b. These scaling relations are now used by ElarmS for all events north of the Gutenberg–Byerly line (shown in Fig. 1 as the line between regions mSA/eCAn and BB/eCAs).

For southern California, Tsang et al. [15] analyzed a dataset of 59 earthquakes recorded by the Southern California Seismic Network (CI) between 1992 and 2003, with magnitudes ranging from 3.0 to 7.3. The analysis resulted in the following scaling relations (Fig. 2c, d):

$$\begin{aligned} M_w &= 6.36 + 6.83 * \log_{10}(\tau_p^{\max}) && \text{for } \tau_p^{\max} \text{ on HHZ, HLZ, HNZ channels} \\ M_w &= 1.24 * \log_{10}(P_d) + 1.65 * \log_{10}(R) + 5.07 && \text{for } P_d \text{ on HH, HL, HN channels} \end{aligned}$$

These scaling relations are used by ElarmS for all events south of the Gutenberg–Byerly line.

Ground motions in Northern and Southern California are predicted using Boatwright et al. [6] GMPE, as preferred by CISN ShakeMap version 3.2 [17]

$$\log_{10}(\text{PGA, PGV}) = A + B * (M - M_s) - \log_{10}(R_g) + k * R + B_v * \log_{10}(V_s/V_a)$$

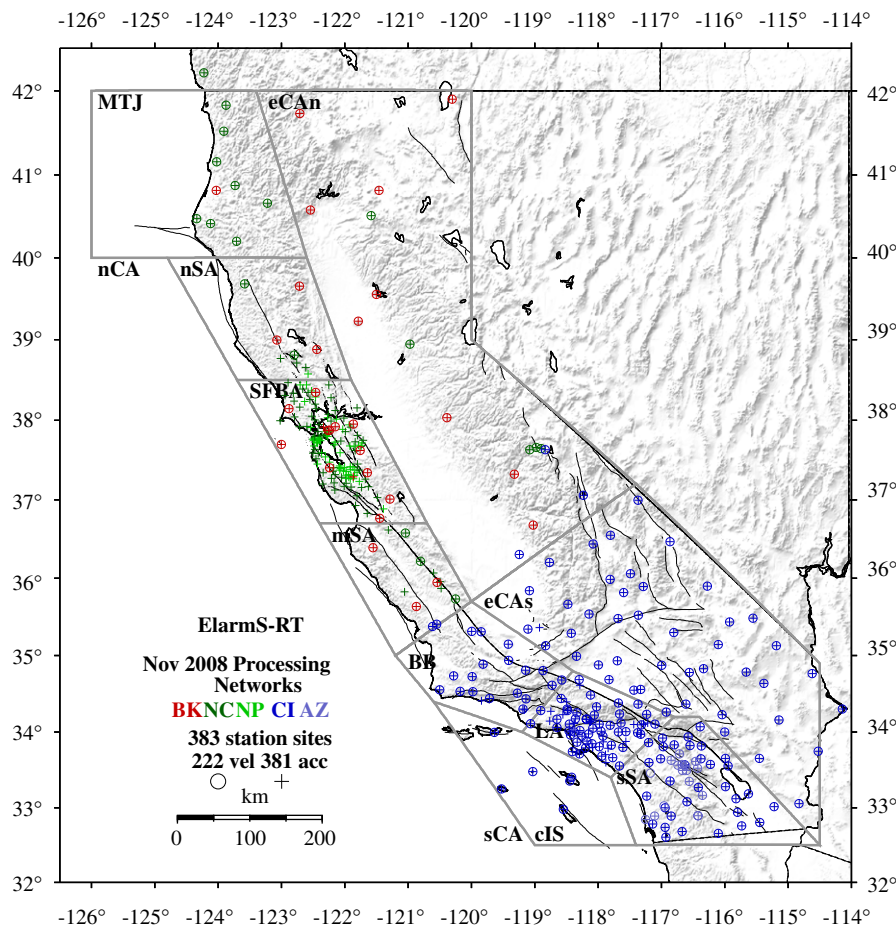


Fig. 1. Realtime seismic stations used by ElarmS in California. Circles are velocity instruments, and crosses are accelerometers. Many stations have co-located velocity and acceleration sensors. The grey boxes indicate regions used for alert requirements: Mendocino Triple Junction (MTJ), north San Andreas (nSA), San Francisco Bay Area (SFBA), middle San Andreas (mSA), Big Bend (BB), Los Angeles (LA), south San Andreas (sSA), Channel Islands (cIS), east California south (eCAs), and east California north (eCAn). The straight line between regions mSA/eCAn and BB/eCAs is the Gutenberg–Byerly line dividing northern and southern California.

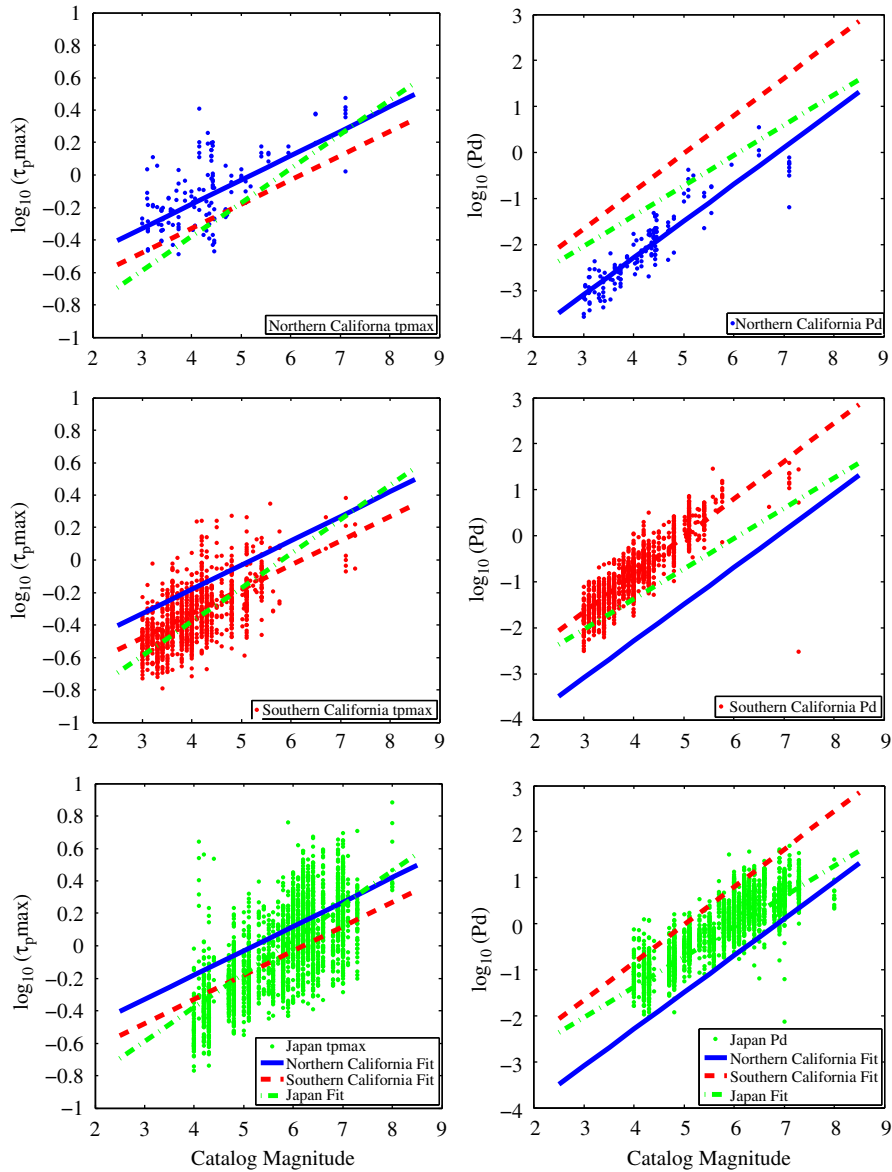


Fig. 2. Scaling relations. (a) τ_p^{\max} , northern California; (b) P_d , northern California; (c) τ_p^{\max} , southern California; (d) P_d , southern California; (e) τ_p^{\max} , Japan; (f) P_d , Japan. Circles are individual station observations of τ_p^{\max} or P_d . Lines are regional scaling relations defined by the linear best fit to the data. The best-fit linear relations for all three regions are shown on all plots.

where M is the event magnitude, V_s is a site correction, $R = \sqrt{R_e^2 + d^2}$, R_e is epicentral distance, d is depth, and $R_g = R$, if $R \leq R_0$, or $R_g = R_0 * (R/R_0)^g$, if $R > R_0$. Remaining coefficients are specific for large events ($M > 5.5$) or small events ($M \leq 5.4$), and are shown in Table 1.

3.2. Realtime processing

ElarmS was adapted to run in realtime in Northern California in October 2007, and expanded statewide in November 2008. The system now processes waveforms from all realtime-capable stations in the state: a total of 603 velocity and accelerations sensors at 383 sites (Fig. 1). The ElarmS waveform processing module is distributed among three regional processing centers, which receive the continuously streamed waveforms. Data from the Berkeley Digital Seismic Network (BK) are streamed to UC Berkeley, data from the Northern California Seismic Network (NC) and from some stations in the USGS Strong Motion Network (NP) are streamed to USGS Menlo

Park, and data from the Southern California Seismic Network (CI), the Anza Network (AZ), and the remaining NP stations are streamed to Caltech/USGS Pasadena. At these regional processing centers, the waveform processing module distills the waveforms to their essential parameters: trigger times, peak predominant period, peak amplitudes (acceleration, velocity, and displacement), peak ground shaking observations, and signal-to-noise ratio. These parameters are then forwarded to UC Berkeley, where a single event monitor integrates data from all of California to identify and analyze earthquakes in realtime. When an event is determined to be above a certain magnitude threshold, an alert message can be sent to users notifying them of the event location, origin time, estimated magnitude, and number of triggers. Currently alerts are sent to the authors and the SCEC database for CISEN EEW analysis.

3.3. System latency

The total ElarmS processing time, from when a P-wave arrives at a station until ElarmS outputs event information, can be divided into

Table 1
Coefficients for the Boatwright et al. [6] ground motion prediction equation used in California.

	<i>A</i>	<i>B</i>	<i>k</i> ₀	<i>R</i> ₀	<i>g</i>	<i>M</i> _s	<i>p</i>	<i>B</i> _v	<i>V</i> _a	<i>k</i>
PGA, <i>M</i> > 5.5	2.52	0.31	−0.0073	27.5	0.7	5.5	0.3	−0.371	560	$k_0 * 10^{(p*(M_s - M))}$
PGV, <i>M</i> > 5.5	2.243	0.58	−0.0063	27.5	0.7	5.5	0.3	−0.371	560	$k_0 * 10^{(p*(M_s - M))}$
PGA, <i>M</i> ≤ 5.4	2.52	1	−0.0073	27.5	0.7	5.5	0	−0.371	560	<i>k</i> ₀
PGV, <i>M</i> ≤ 5.4	2.243	1.06	−0.0063	27.5	0.7	5.5	0	−0.371	560	<i>k</i> ₀

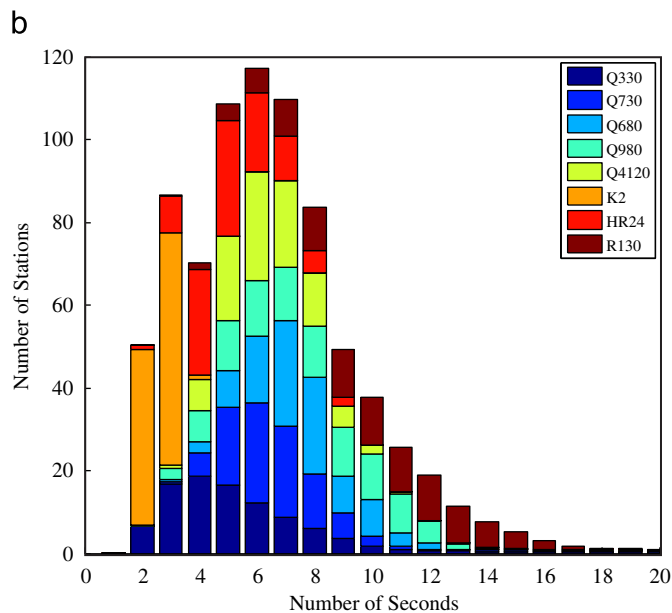
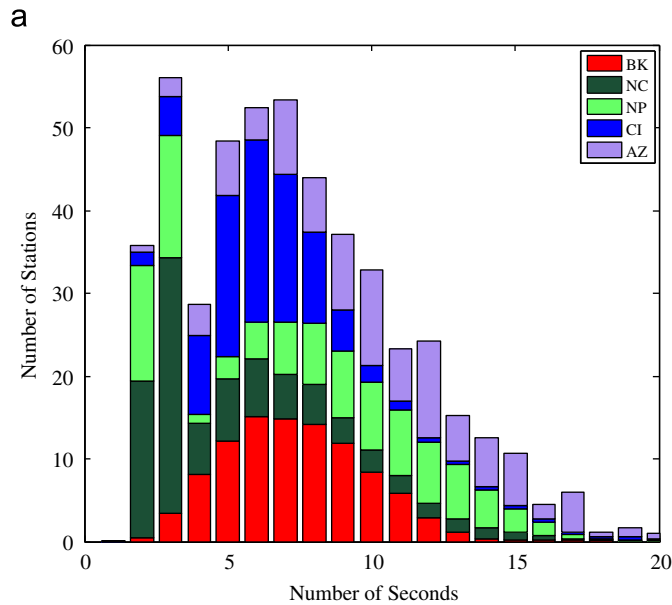


Fig. 3. A stacked histogram of latencies by (a) network, and (b) data logger type. Both histograms are truncated at 20 s for clarity, but the long tail to the histogram continues, with columns of 0–2 data points, up to as much as 200 s.

two types: telemetry of data and computer analysis time. Data telemetry includes the time while a station collects data into a packet for transmission, transit from individual stations to the regional processing centers where the waveforms are processed, and transit time from the processing centers to UC Berkeley where the single event monitor is located. Stations transmit data to the processing centers by frame-relay, internet, private intranet, radio,

Table 2
Median values for the telemetry latencies shown in Fig. 3.

	Median delay (s)
Network	
BK	6.2
NC	2.5
NP	7.4
CI	5.2
AZ	9.3
Data logger	
Q330	4.0
Q730	5.5
Q680	6.3
Q980	6.6
Q4120	5.3
K2	1.6
HR24	4.0
R130	9.1

or microwave, depending on the station. The processing centers transmit data to Berkeley by internet or private intranet.

The primary source of telemetry latencies is the packetization of data by station data loggers. A data logger will not send its data to the waveform processing module until the data packet is full. Packet sizes are usually of a configurable byte size, but many station data loggers are currently set for packet sizes equivalent to 4–6 s of data. Manually reconfiguring these data loggers to require packets equivalent to 1–2 s of data would greatly decrease the delays. In addition, all BK data loggers and most CI data loggers will be upgraded to data loggers with short 1 second packets in the next two years with recently provided US Federal stimulus funding as part of the American Recovery Reinvestment Act (ARRA).

Fig. 3a shows the data latencies for transmission to the waveform processing site by each seismic network. These delays are the difference in seconds between when a P-wave arrives at a station and when the waveform packet is received by the regional processing center. They are thus composed of the time for a packet to fill and the time in transit to the regional processing center. The median latencies for each network are shown in Table 2. The median latency across all networks is 5.23 s. Each histogram is characterized by an extended tail at the high latencies (the figure is truncated at 20 s for clarity, but the distributions continue to higher latencies, up to several hundred seconds, for a small number of stations). The tail indicates stations that are drastically delayed, due to poor telemetry availability, temporary telemetry failure or station disruption.

NC has the fastest median of 2.5 s due to a large number of NC station data loggers configured for a packet size equivalent to 1–2 s of data. However, there is a substantial tail to the distribution, indicating that the remaining stations are significantly slower. The Gaussian-like distribution for BK, with a median of 6.2 s, illustrates the nearly uniform hardware, software and telemetry configuration for all stations in the network, with few excessively delayed stations. CI uses much the same

equipment as BK and shows a similar distribution with a slightly faster median of 5.2 s. NP is a little slower with a median of 7.4 s. The NP distribution shows a peak around 2 or 3 s, similar to NC, but a multitude of slower stations add a significant tail to the distribution, increasing the median. AZ has the highest median latency, 9.3 s, which is due to an extra telemetry step as the data is forwarded through the Scripps Oceanographic Institute before arriving at the Caltech regional processing center.

Fig. 3b shows the delays by data logger type, independent of network. Again, the delays are the difference between when a P-wave arrives at a station and when the waveform packet is received by the regional processing center. The distribution statistics are shown in Table 2. The fastest data logger is the K2 used at many of the USGS sites and designed to send 1 s data packets. The Quanterra Q330 comes second, again due to the fact that it sends out 1 s data packets, although there is a wider range of the total telemetry latencies which is likely due to software discrepancies between the different networks. The Berkeley processing software was designed for the older model data loggers and has not yet been updated to accommodate the Q330. This software will be upgraded by Spring 2010. The older Quanterra data loggers (the Q730, Q680, Q980, and Q4120) are slower. In the network upgrade that is now underway the majority of these older and slower data loggers are being upgraded to Q330s. The combined effect of new data loggers and revised software will reduce the latencies at these stations by 3 to 5 s.

3.4. Alert criteria

The station distribution in California is not uniform (Fig. 1). Not surprisingly, the performance of a network-based system is directly related to the density of the network. Accuracy improves when more stations contribute to an event estimate, but potential warning time is lost while waiting for those stations to trigger, especially when the stations are far apart. ElarmS performs best in the heavily instrumented regions around Los Angeles, San Diego, and San Francisco (LA, sSA, SFBA in Fig. 1). In these regions the mean station separation is only 20 km, and the system often receives two or three triggers in the first second after an earthquake begins. In regions with lower station density the system must wait, as valuable seconds pass, until enough stations have reported P-wave arrivals. Regions with less dense instrumentation also suffer from higher false alarm rates, as there are fewer stations to contradict a false trigger. We therefore tailor the alert requirements to each region.

In regions SFBA, LA and sSA, where inter-station spacing is approximately 20 km, the system requires at least 4 triggers within 30 km of the epicenter before an alert can be sent for an event. In southeastern California (eCAs), the Big Bend region (BB), the middle San Andreas (mSA), and the northern San Andreas (nSA), where stations are separated by 20–100 km, we require 5 or more stations within 100 km to trigger before an alert is generated. And in the Mendocino Triple Junction (MTJ), north-eastern California (eCAn), and the Channel Islands (cIS), where stations are more than 100 km apart, we require 10 or more stations (at any epicentral distance) to trigger. These regional boundaries and requirements continue to be refined as we monitor the realtime system.

3.5. False and missed alerts

Fig. 4 shows all detected, false, and missed alerts with magnitude 3 or greater that occurred in Northern California during a ten-week test period from 8 August 2009 and 20 October

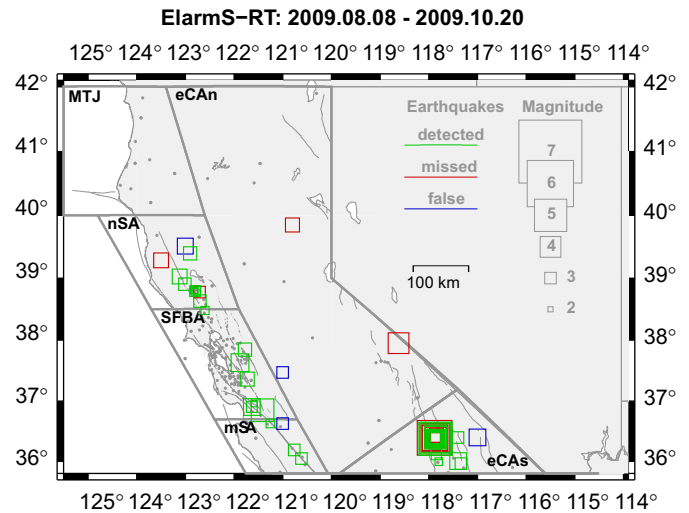


Fig. 4. Map showing all ElarmS-detected earthquakes with $M > 3$, and all false and missed alerts in Northern California, during a ten-week test period from 8 August 2009 until 20 October 2009. Green, red, and blue boxes are detected, missed, and false alerts, respectively. Grey dots are seismic stations. (For interpretation of the references to colour in this figure legend, the reader is referred to the web version of this article.)

2009. A false alert is defined as an ElarmS event that meets the alert criteria for its region but does not correspond to an event in the Advanced National Seismic System (ANSS) catalog. A missed alert is an ANSS $M > 3$ event for which no ElarmS alert message was issued; ElarmS may have not detected the event, or it may have detected the event but not satisfied the criteria required to issue an alert. For this ten-week test period there were 63 real events $M > 3$. ElarmS detected 45 of them and missed 18. Eleven of the missed events were part of an aftershock sequence described below. ElarmS also sent four false alert messages for nonexistent events.

The false and missed alarm rates are related to two factors: the station density, and whether an earthquake is occurring during a swarm such as during an aftershock sequence. In the SFBA region, where inter-station spacing is approximately 20 km, there were 8 detected events and no false or missed alerts for this time period (Fig. 4). In mSA there were 3 detected events and 1 false alert. In nSA there were 8 detected events, 1 false alert and 2 missed alerts. Performance is moderate in the mSA and nSA regions as the station spacing is 20–100 km.

In the eCAn and eCAs regions performance is much poorer due to the much lower station density. In eCAn there were two missed alerts and one false alert. In the eCAs region in the lower right of the map there is a cluster of green (detected) and red (missed) squares. These represent two $M5$ events on October 1st and 3rd, and their aftershock sequences. ElarmS successfully detected the $M5.1$ event on October 1st, but missed the $M5.2$ event two days later. It caught 20 out of 31 total aftershocks of magnitude 3 or greater. ElarmS missed the second large event due to increased background noise and concurrent aftershock activity from the first event.

This illustrates the challenge of defining optimal alert criteria for each region. Criteria which are too strict (requiring too many stations to trigger) may fail to be met by a moderate size event, resulting in no alert message even though the event is real, or will slow down the time until an alert is issued. Criteria which are too loose (requiring too few stations) may be met by unrelated, erroneous triggers, resulting in an alert message when there is no real event. As with all associators the performance is also reduced during swarms of seismicity or aftershock sequences.

Improvements to the associator scheme specifically for early warning applications would be beneficial.

4. Sample events

We illustrate ElarmS performance in California with three sample events from different regions of the state, all processed by the realtime system.

4.1. M_w 5.4 Alum Rock, SFBA region

Fig. 5 shows the M_w 5.4 Alum Rock event, which occurred on 30 October 2007. This was the largest event in the San Francisco Bay Area since the 1989 Loma Prieta M_w 6.9 event. At the time of the Alum Rock earthquake, ElarmS had been running in realtime for less than a month and used only stations from the BK network. The event begins in Fig. 5a when two stations trigger simultaneously. The location is estimated between the stations, at a depth of 8 km. One second later (Fig. 5b), the magnitude is estimated at 5.2, using the observed τ_p^{\max} and $P_{d/v}$ values from the two triggered stations. A third station triggers and the location is triangulated based on the arrival times at the three stations. The estimated location and magnitude are applied to local GMPEs to produce a prediction of ground shaking around the epicenter. The mean errors in the PGA and PGV predictions are -0.2 and -0.3 , respectively, at this time. PGA and PGV errors are the difference of the logarithm of the observed minus the predicted ground motions; a factor of two difference between the predicted and observed PGA corresponds to an error of 0.7, and a factor of 10 to

an error of 2.3. One second later (Fig. 5c), the τ_p^{\max} and $P_{d/v}$ values from the third station are incorporated, and the magnitude estimate rises to $M5.8$. The errors in PGA and PGV change to 0.0 and -0.4 . One second later (Fig. 5d), a fourth station triggers, the location is adjusted, and the magnitude estimate rises to $M5.9$. The predictions of peak ground shaking are adjusted to account for the new location and magnitude estimates and a second peak ground motion observation. The mean PGA and PGV errors change to 0.1 and -0.2 . As additional seconds pass, more stations trigger and their P-wave parameters are incorporated into the evolving estimates of location and magnitude, and the predictions of ground shaking. Figs. 8a and b show the errors in the magnitude and location estimates as time progresses.

ElarmS uses a bias correction to shift the GMPEs up or down to match available ground motion observations. In Fig. 5c the AlertMap shows a decrease in expected ground motions, despite the increase in magnitude. In this case there is only one observation available (represented by the light blue diamond just southeast of the epicenter), and it lowers the predictions for the whole region until more observations are available in the next second. Iervolino et al. [12] found that GMPEs contribute significantly more error to EEW predictions of ground shaking than do magnitude or location estimates. This is due to the inherent variability in peak ground motion at a given location with respect to even the best fitting attenuation relations. However, Iervolino et al. [12] also found that ground motion predictions stabilize as more information is incorporated. While the inclusion of a single ground motion observation may increase the error in the AlertMap [9], as more observations are included their individual errors cancel each other out. Future versions of ElarmS will wait until three or more ground

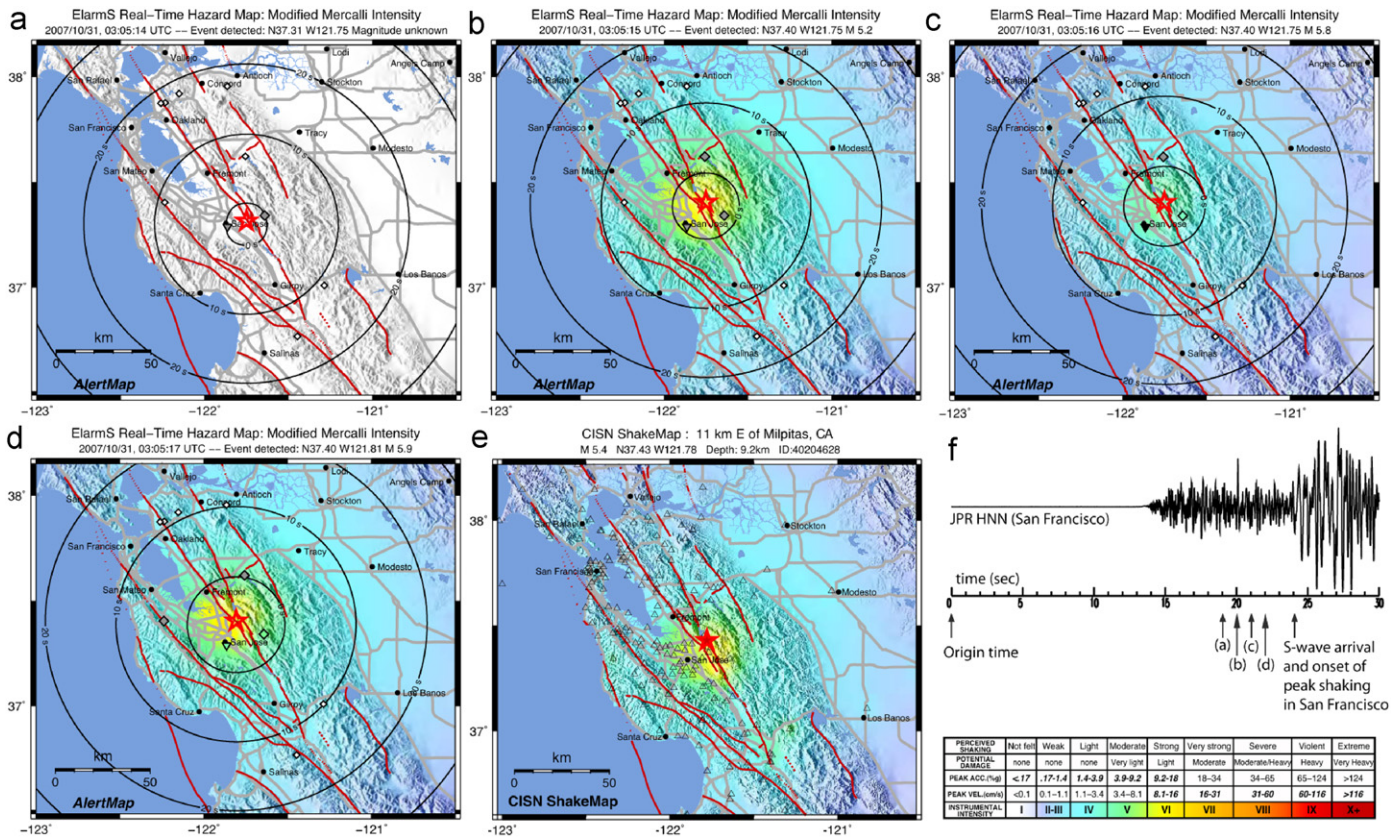


Fig. 5. Example of ElarmS event processing for the 30 October 2007 Alum Rock M_w 5.4 earthquake. (a–d) Progressive AlertMaps as stations trigger and the event is analyzed in realtime. The AlertMaps themselves were produced after the event, but the data used to create them was available at the time indicated on the map. (e) CISM ShakeMap published after the event. (f) Timeline comparing when the data used to create the AlertMaps was available with respect to the arrival of peak ground shaking in San Francisco.

motion observations are available before including them in the prediction, to avoid the increased uncertainty associated with using just one or two observations.

Fig. 5e shows the CISM ShakeMap published after the Alum Rock event. From the time of the first magnitude estimate, one second after the first P-wave detection, the predictive AlertMap (Fig. 5b) is a close match to the ShakeMap. Fig. 5f shows a seismogram recorded in San Francisco during the Alum Rock earthquake. The timeline denotes the times at which the data used in (a), (b), (c), and (d) was available. At the time ElarmS applied a 15 s buffer to the incoming waveforms, to reduce latency differences between stations. Despite the 15 s buffer, the data used to create (b–d) was available four to two seconds before the S-waves reached San Francisco and peak ground shaking began. This event represented the first “proof-of-concept” event for the realtime ElarmS system as it illustrates that hazard information is available before shaking is felt.

4.2. $M_w5.4$ Chino Hills, LA region

Fig. 6 shows the $M_w5.4$ Chino Hills event, which occurred on 29 July 2008. At the time ElarmS was midway through the conversion to statewide coverage, and was receiving data from only 15 southern California stations. ElarmS was still able to estimate magnitude, location, and ground shaking using only the three stations within 100 km of the epicenter. When the first station triggered, the event was located directly beneath the station at a depth of 8 km. The observed τ_p^{max} and $P_{d/v}$ values were used to estimate a magnitude of 5.4. From that location and magnitude, local GMPEs were used to predict peak ground shaking in the region (Fig. 6a). After a second station triggered, the location was adjusted between the stations based on arrival times, at a depth of 8 km. The τ_p^{max} and $P_{d/v}$ magnitudes for the second station were averaged together with those from the first station, producing a new event magnitude of $M5.8$. The new location and magnitude were used to update the predictions of ground shaking (Fig. 6b). Fig. 6c shows the CISM ShakeMap for comparison. The ShakeMap is published after the event, using observations from all available stations. The ElarmS predictive AlertMap is reasonably similar to the ShakeMap, considering ElarmS used data from only two stations (the third and final available station triggered six seconds later and did not

significantly change the AlertMap). Figs. 8c and d show the progression of magnitude and location errors with time.

4.3. $M_w4.4$ Lone Pine, eCAs region

The Lone Pine $M_w4.4$ occurred on October 3, 2009, in the eCAs region. In this region the stations are separated by 20–100 km, so ElarmS requires at least 5 stations to trigger before issuing an alert. In Fig. 7a the event is detected when two stations trigger simultaneously, four seconds after the event origin time. One second later (7b) the event magnitude is estimated at 4.0. Four more seconds pass before a third station triggers, at which point the location is adjusted and the magnitude estimate is raised to 4.1 (7c). The thin station coverage necessitates waiting longer in this region than in the previous examples. The five station requirement for alert issuance is not met until two seconds later (7d), 11 seconds after the event begins. The fourth and fifth stations did not appreciably change the magnitude, location, or ground motion predictions in this case, but they ensured that the event was real (Fig. 8e, f).

5. Application of ElarmS to Japan

5.1. Scaling and GMPEs

While ElarmS has been tested with many datasets in California, there are few recent, well-recorded, large earthquakes in California. Since an early warning system is designed specifically to warn people of large events, we are especially interested in its performance for these events. Thus we tested the system with a dataset of large events from Japan [9]. The Japanese events also provided insight into ElarmS’ performance in a subduction zone environment.

The dataset included 84 Japanese events that occurred between September 1996 and June 2008 (Fig. 9). The magnitudes ranged from 4.0 to 8.0, with 43 events of magnitude 6.0 or greater. The largest event was the M8.0 Tokachi-Oki earthquake of 26 September 2003. The events were recorded by Japan’s Kyoshin Net (K-NET) strong-motion seismic network. K-NET consists of 1000 digital strong motion seismometers, distributed across Japan with approximately 25 km spacing. Each station is capable of recording

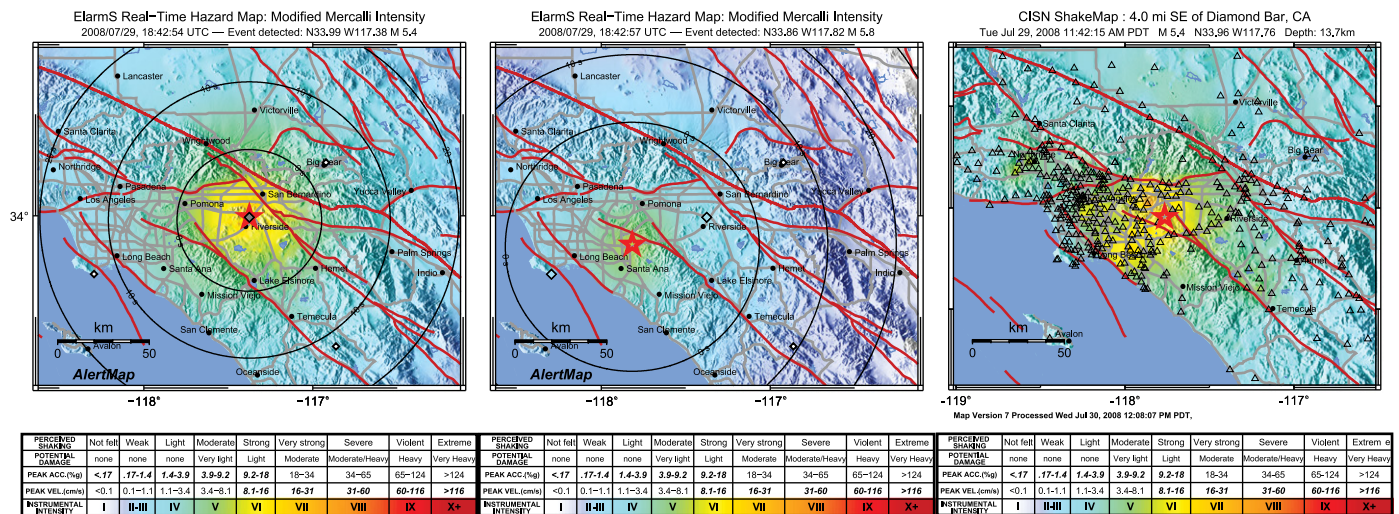


Fig. 6. Example of ElarmS processing for the 29 July 2008 Chino Hills $M_w5.4$ earthquake. (a) AlertMap showing predictions of ground shaking after one station had triggered. (b) AlertMap showing adjusted predictions after two stations had triggered. (c) CISM ShakeMap published after the event.

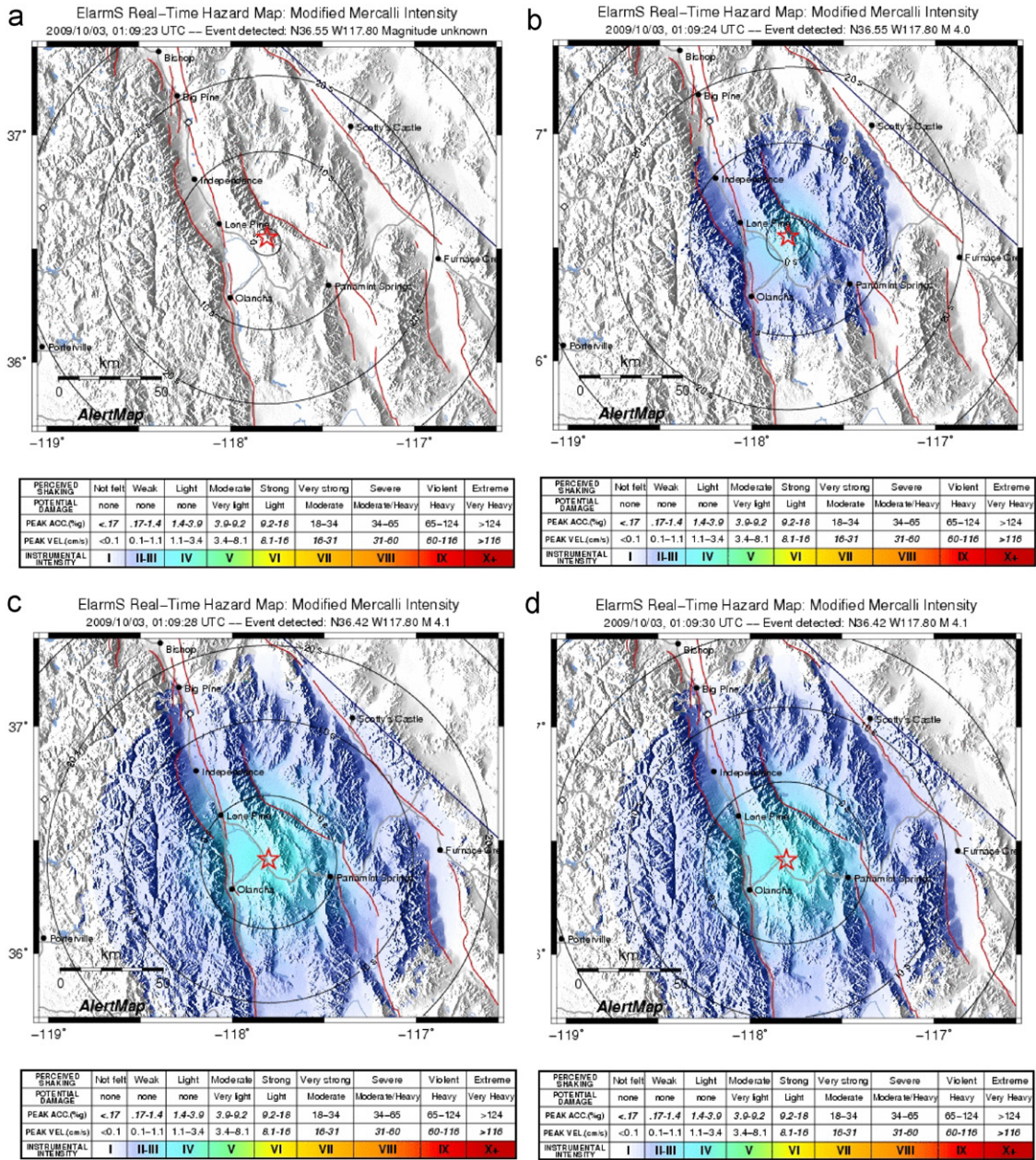


Fig. 7. Example of ElarmS processing for the 3 October 2009 Lone Pine M_w 4.4 earthquake. (a) Hypocenter was estimated when two stations triggered, 4 s after the event began. (b) One second later (OT+5 s) magnitude was estimated at 4.0, using P-wave parameters from the two triggering stations. (c) Four seconds later (OT+9) a third station triggered. Location, magnitude, and ground shaking predictions were adjusted. (d) One second later (OT+11), the five station requirement was met and an alert was issued (to the authors) for this event.

accelerations up to 2000 cm/s^2 , with a sampling frequency of 100 Hz and a dynamic range of 108 dB.

The events were processed offline, using all available data, using the same methodology as described above. The first step is to determine scaling relations between the predominant period and peak amplitudes of the P-waves and the magnitude for the event dataset. The observed scaling relations for Japan are shown in Fig. 2e, f and are

$$M_{JMA} = 4.76 * \log_{10}(\tau_p^{\max}) + 5.81$$

$$M_{JMA} = 5.82 + 1.52 * \log_{10}(P_d) + 1.39 * \log_{10}(R)$$

where M_{JMA} is the JMA catalog magnitude and R the epicentral distance. The predominant periods observed in Japan are of similar values to those of Northern and Southern California,

but the best-fit slope is steeper in Japan. The peak amplitude values are higher than those in Northern California and lower than those in Southern California, with a slightly shallower slope in Japan.

For the prediction of peak ground shaking, we used the GMPEs that the global ShakeMap system uses for Japanese events. The global ShakeMap GMPEs use either the Boore et al. [7] or the Youngs et al. [19] model, depending on depth and magnitude of the event. For events shallower than 20 km or smaller than magnitude 7.7, the relations are defined by Boore et al. [7], with numerical coefficients specified for reverse faulting

$$\ln(PGA) = -0.117 + 0.527 * (M - 6) + 0.778 * \ln(R)$$

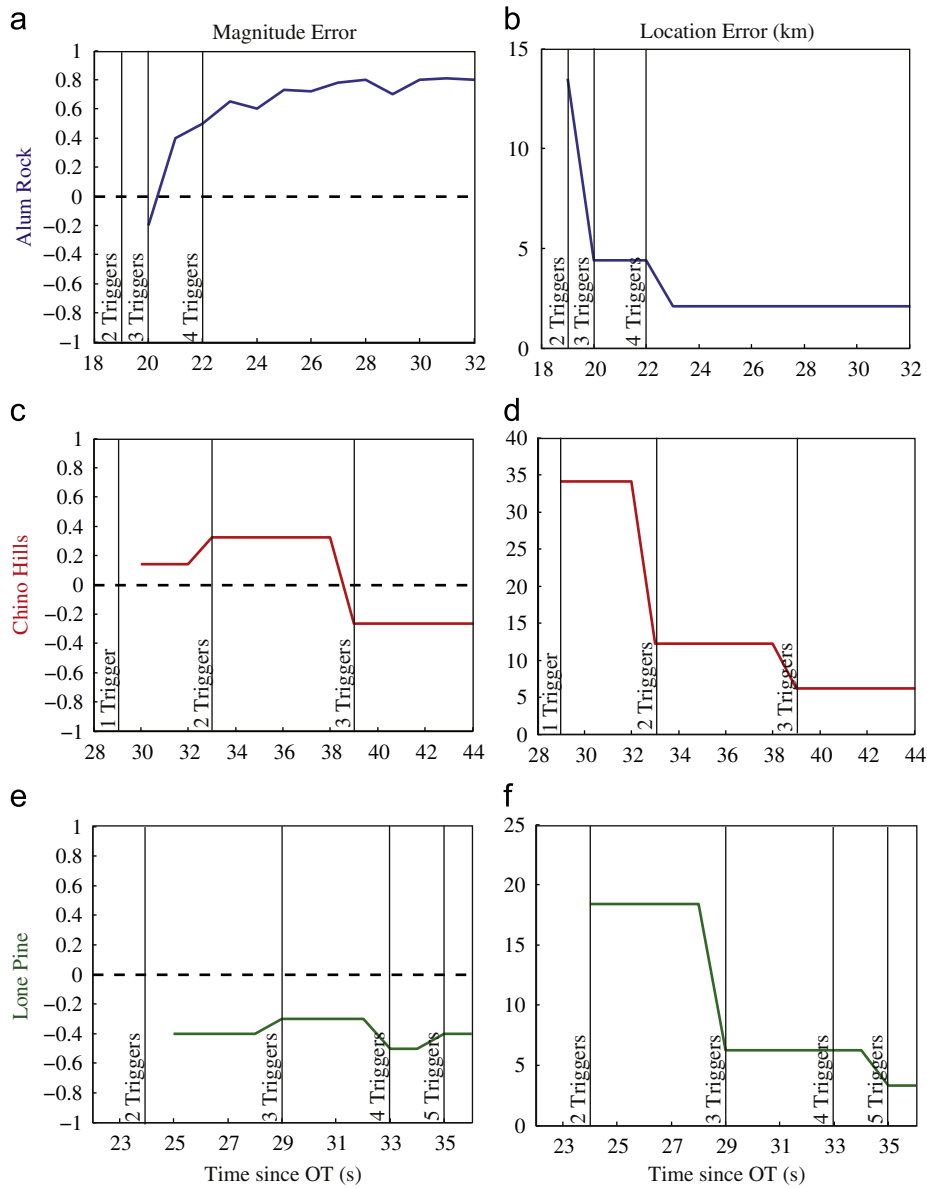


Fig. 8. Magnitude and location error with time for the three California sample events: Alum Rock (a, b), Chino Hills (c, d), and Lone Pine (e, f). Horizontal axis is time in seconds since origin time of the earthquake. These times include a 15-second buffer for Alum Rock and 20-second buffers for Chino Hills and Lone Pine. Vertical axis is error in magnitude estimate (magnitude units) or epicentral location estimate (km).

where R is defined by

$$R = (R_{jb}^2 + h^2)^{1/2}$$

R_{jb} is the closest distance in km to the surface projection of the fault and h is a model coefficient representing depth. We substitute the epicentral distance for R_{jb} .

For events deeper than 20 km or greater than magnitude 7.7, global ShakeMap and ElarmS use the GMPEs defined by Youngs et al. [19]

$$\ln(\text{PGA}) = 0.2418 + 1.414 * M - 2.552 * \ln(R_{jb} + 1.7818 \exp(0.554 * M)) + 0.00607 * h$$

where again we substitute the epicentral distance for R_{jb} .

5.2. Performance for large magnitudes

Once the necessary scaling relations had been developed all 84 events were processed in a simulated realtime environment to provide ElarmS predictions of ground shaking. We assumed zero

data latency and processed data sequentially according to the time-stamp on the waveform data. After the events were processed we analyzed ElarmS performance for different magnitude ranges. Fig. 10 shows the resulting ElarmS magnitude histograms. The blue histogram is the magnitude error for all events in the Japanese dataset, with magnitudes from 4.0 to 8.0. The mean error for all events was 0.0 magnitude units, with a standard deviation of 0.4. The green histogram is the magnitude error for all events magnitude 6.0 or greater (of which there are 43). The mean error for this distribution is again 0.0, with a standard deviation of 0.5. This is a similar distribution statistically to that for all events. The red histogram is the magnitude error for events magnitude 7.0 or greater (of which there are seven in this dataset). Of the seven events $M > 7$, four of the magnitudes are underestimated, two are overestimated, and one is accurately estimated. The mean error for this distribution is -0.2 magnitude units, with a standard deviation of 0.5. This lower mean error means that ElarmS underestimates the magnitude of the largest

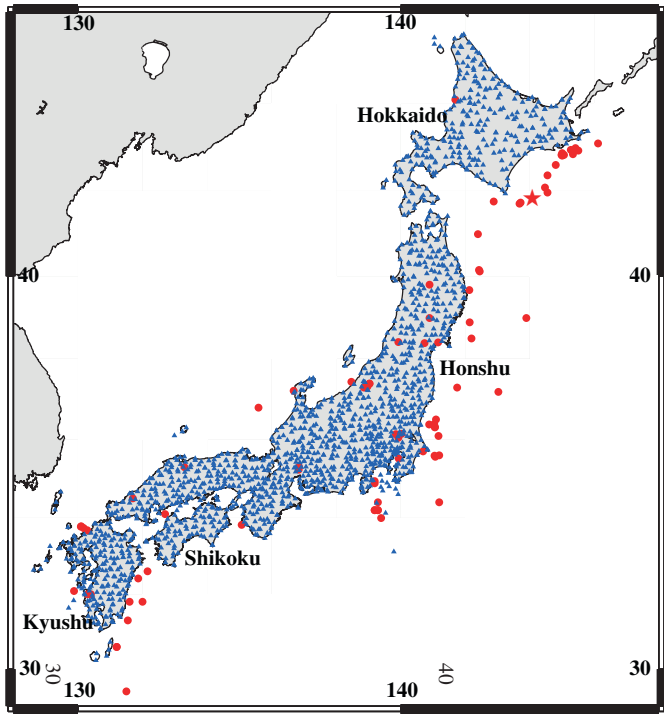


Fig. 9. Events and stations used in the Japan test dataset. Red circles are events, blue triangles are K-NET stations. The red star is the largest event in the study, the M8.0 Tokachi-Oki earthquake of September 26, 2003. (For interpretation of the references to colour in this figure legend, the reader is referred to the web version of this article.)

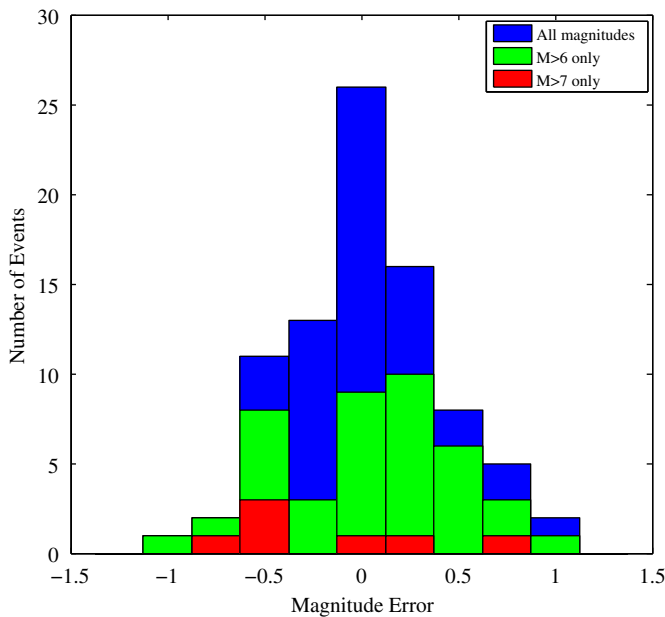


Fig. 10. Histogram of magnitude errors for Japan dataset. The blue histogram is the distribution of magnitude error for all 84 events in the Japan dataset, M4.0 to M8.0. The green histogram is the distribution for the subset of 43 events with magnitude 6.0 or greater (up to and including magnitude 8.0) and overlays the blue histogram. The red histogram, again overlaying the green histogram, is for the subset of 7 events with magnitude 7.0 or greater (up to and including magnitude 8.0). (For interpretation of the references to colour in this figure legend, the reader is referred to the web version of this article.)

events by 0.2 magnitude units on average. An underestimation of 0.2 magnitude units is within our tolerance for ElarmS magnitude estimates, but we recognize that the magnitude algorithm may

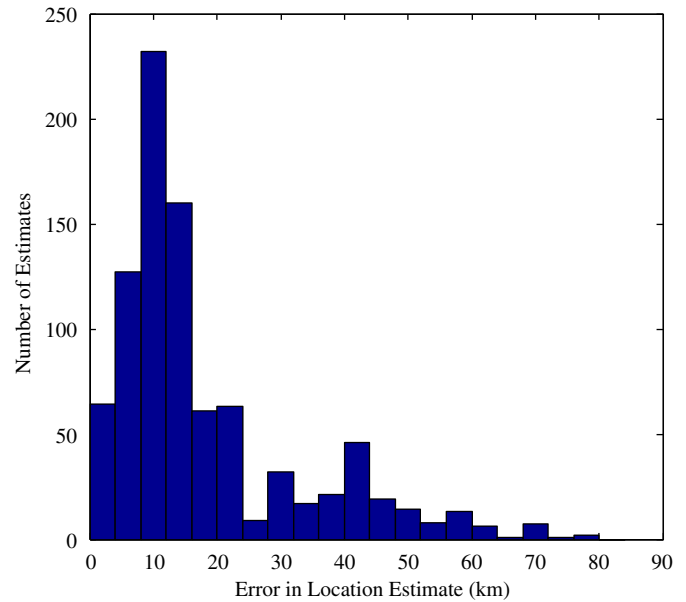


Fig. 11. Histogram of location errors for Japan dataset. Each event contributes an initial 1-trigger estimate, a 2-trigger estimate, and so on until all available stations are included. The median error across all estimates, with any number of triggers, is 11 km.

need to be adjusted to prevent underestimation in the future. A first step may be to weight the average of τ_p^{\max} and $P_{d/v}$ in favor of τ_p^{\max} for high magnitude events, since τ_p^{\max} is less prone to saturation effects at the highest magnitudes [9].

5.3. Methodological improvements

The Japanese dataset provided some methodological challenges. The majority of the events were offshore. The resulting limited azimuthal coverage (all stations are onshore) slowed down our location algorithm, requiring more station trigger times and therefore more seconds to produce a reasonable epicentral estimate. Many of the events were also deep. The original California location algorithm assumed a depth of 8 km for all events, and found the hypocenter on a 2D grid at that depth. For the subduction zone events we expanded the algorithm into a 3D grid search, finding hypocenters at depths down to 80 km, in 10 km increments. Fig. 11 shows a histogram of location estimate errors using the new 3D grid search. The histogram includes all hypocentral location estimates for each event, from the initial 1-trigger estimate to the final estimate using all available stations. The median location error, across all events and all number of triggers, is 11 km.

5.4. Error model

As part of the Japan dataset testing, we developed an error model similar to that of Iervolino et al. [12], to analyze the errors in ElarmS' output [9]. We separated the algorithm into its location, magnitude, and ground motion steps, and isolated the errors produced during each step. Errors were calculated by comparing the estimated location or magnitude to the catalog location or magnitude, and the predicted ground shaking at all stations and times prior to recording ground shaking to the eventual observation of peak ground shaking at that station. Predictions of peak ground shaking at stations after the peak shaking had occurred were not included in the error analysis. The errors of each component of the system are shown in Table 3.

Table 3
Parameters (mean and standard deviation) of error distributions for magnitude, location, and ground motion.

	0 stations	1 station	2 stations	3 stations	4 stations	5 stations
Mag, 1 sec	–	−0.4 ± 0.6	−0.3 ± 0.6	−0.4 ± 0.6	−0.4 ± 0.6	−0.4 ± 0.6
Mag, 2 sec	–	−0.2 ± 0.6	−0.2 ± 0.5	−0.2 ± 0.5	−0.2 ± 0.5	−0.2 ± 0.5
Mag, 3 sec	–	−0.1 ± 0.5	−0.1 ± 0.5	−0.1 ± 0.5	−0.1 ± 0.5	−0.1 ± 0.5
Mag, 4 sec	–	0.0 ± 0.5	0.0 ± 0.5	0.0 ± 0.5	0.0 ± 0.4	0.0 ± 0.4
Mag, 5 sec	–	0.0 ± 0.5	0.1 ± 0.4	0.1 ± 0.5	0.1 ± 0.4	0.1 ± 0.4
Location	–	34 ± 18	32 ± 21	32 ± 19	19 ± 14	21 ± 17
PGA	0.1 ± 0.3	0.1 ± 0.4	0.1 ± 0.4	0.1 ± 0.3	0.1 ± 0.3	0.0 ± 0.3

The accuracy of any given step is dependent on the amount of data available. The error in the location estimate, for example, is dependent on the number of stations reporting P-wave arrivals. The error in the magnitude estimate is dependent on both the number of stations providing information and the number of seconds of P-wave that have arrived at each station. The error in the prediction of peak ground shaking is dependent on the number of stations whose observations of peak ground shaking have been used to adjust the prediction. The “0 stations” error is when no stations have yet recorded peak ground shaking, and the prediction of ground shaking is based on the GMPEs alone.

The errors calculated (Table 3) were then used to produce an error model for ElarmS’ final prediction of ground shaking, given any combination of inputs. If there were no errors at all in the system, then the ElarmS prediction of ground shaking would be based on the same magnitude and location that the catalog uses. Since ElarmS uses the global ShakeMap GMPEs, an error-free ElarmS AlertMap should look much like the global ShakeMap. Therefore, the error contributed by ElarmS is the difference between the ShakeMap calculation of ground shaking and the AlertMap prediction of ground shaking. The ideal, error-free output is defined by the GMPEs for an event. For example, for an event shallower than 20 km depth with a magnitude less than 7.7, the error-free output would simply be the Boore et al. [7] GMPE. For peak ground acceleration (PGA)

$$\ln(\text{PGA})_{\text{ideal}} = -0.117 + 0.527*(M-6) + 0.778*\ln(R) \text{ ideal, error-free output}$$

where M is magnitude and R the distance from the event epicenter to the location where PGA is being predicted.

We then introduce errors into the calculation, using the error distributions we observed for our Japan dataset.

$$\ln(\text{PGA}) = -0.117 + 0.527*(M + \epsilon_M - 6) + 0.778*\ln(R \pm \epsilon_R) + \epsilon_{\text{Att}} \text{ ElarmS output}$$

where M is the catalog magnitude, R is the epicentral distance, and ϵ_M , ϵ_R , and ϵ_{Att} are the errors in magnitude, location, and GMPEs, respectively.

The difference between PGA_{ideal} and \hat{PGA} is the error in our final prediction of ground shaking.

$$\epsilon_{\text{PGA}} = \ln(\text{PGA})_{\text{ideal}} - \ln(\hat{PGA}) \text{ Error}$$

This represents the total error in the entire algorithm. ϵ_{PGA} is a unitless value; a factor of two difference between the ideal and estimated PGA corresponds to an error of 0.7, and a factor of 10 to an error of 2.3.

The errors for each step (ϵ_M , ϵ_R , ϵ_{Att}) are dependent on the quantity of data included (the number of trigger times, the number of τ_P^{max} and $P_{d/v}$ values, etc.) and vary within the probability distributions defined in Table 3. Thus the error model is similarly dependent. We calculated ϵ_{PGA} 1000 times for every combination of data inputs, 1086 combinations, each time choosing the error values by a Monte Carlo simulation based on the mean and standard deviation of the error distributions (Table 3). The resulting 1000 values for ϵ_{PGA} are used to create a probability distribution for ϵ_{PGA} given that specific combination of

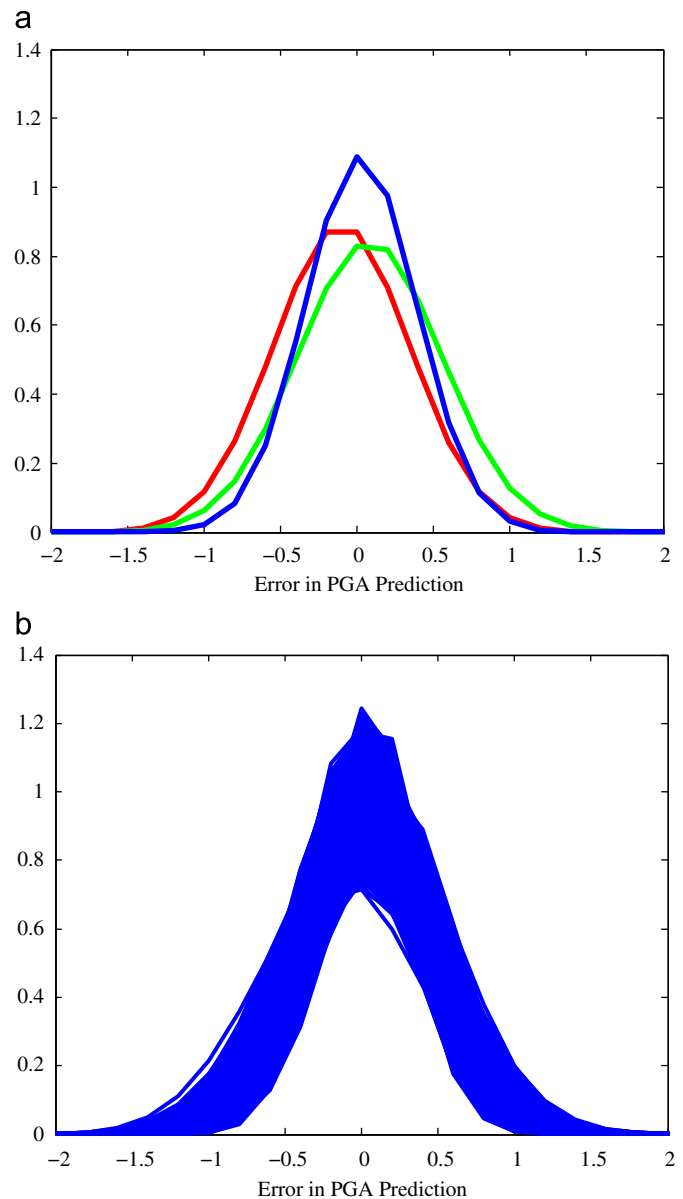


Fig. 12. Error model distributions. (a) Three examples, showing best-fit Gaussian distributions for errors in ground motion estimation, given various quantities of data input. The red line is the error if two stations contribute to a location estimate, two stations contribute to the magnitude estimate (one using 1 s of P-wave data, one using 2 s), and zero stations report PGA observations. The green line is error if three stations contribute to the location estimate, two stations contribute to the magnitude estimate (one with 2 s of P-wave data, one with 3 s), and one station reports a PGA observation. The blue line is error if five stations contribute to the location estimate, five stations contribute to the magnitude estimate (4 with four seconds of P-wave data, one with 3 s), and three stations report PGA observations. (b) All 1086 error distributions resulting from the error model. Each line represents a unique combination of data inputs.

data inputs. Fig. 12a shows three sample ε_{PGA} distributions, and Fig. 12b shows all 1086 ε_{PGA} distributions, corresponding to 1086 unique combinations of data inputs (number of stations contributing to location estimate, number stations contributing to magnitude estimate, number of seconds of P-wave for each station, and number of observations of peak ground shaking). The mean errors for all ε_{PGA} distributions range from -0.2 to 0.2 , with a median of 0.0 . Standard deviations range from 0.3 to 0.6 , with a median of 0.4 . The standard deviations of all error distributions are less than 0.7 meaning less than a factor of 2 error in the PGA prediction. These calculated error distributions are stored in an internal library, accessible during processing for realtime estimates of uncertainty in PGA predictions.

Finally, we analyzed the error contributions of each step of the algorithm separately. By assuming zero error in the magnitude estimate, for example, we could remove that error contribution from the system and observe how much the 1086 error distributions change. In all cases the error distributions remained centered about zero, but the median standard deviation decreased, indicating a decrease in the range of errors. Removing the GMPE error from the system (by setting $\varepsilon_{\text{Att}}=0$) decreased the median standard deviation by 49%, compared with a decrease of 13% when location error was removed ($\varepsilon_{\text{R}}=0$) and 5% when magnitude error was removed ($\varepsilon_{\text{M}}=0$) [9]. This result confirmed that of Iervolino et al. [12], who demonstrated conclusively that GMPEs contribute the most uncertainty to an EEW prediction of ground shaking. Iervolino et al. [12] also showed that predictions of peak ground motions only stabilize when data is included from multiple stations. Since an EEW must use GMPEs, the safest recourse is to wait until multiple stations are providing data before issuing a prediction of ground motions. As always, there is a trade-off of speed versus accuracy in any EEW prediction [12].

6. Conclusion

The three-year CISN project gave us the opportunity to combine the offline development of ElarmS in California with the error analysis performed in Japan and produce a statewide realtime system. Already we have integrated data from five disparate networks, adapted our algorithms to run in realtime using data that is unevenly delayed by telemetry, and added the ability to send alert messages within seconds of event detection. While improvements to the seismic networks in California would improve ElarmS performance, ElarmS has successfully predicted ground shaking for many events even with the current network of stations.

There are opportunities for improvement in the next three-year phase of the project. Our algorithm continues to struggle with false alarms, especially in the regions with low station density. Honing our regional trigger requirements may be the primary step needed to reduce the false alarm rate. In addition, the event associator needs to be improved to better tolerate aftershock sequences, so that we do not risk missing a large mainshock due to its foreshock or other nearby events.

Data latencies are also a significant problem, claiming much of the potential warning time. Some latencies may be reduced by more efficient code design, such as updating the BK network software to accommodate the faster Q330 data loggers. Others

require reformatting individual station data loggers, or upgrading data logger hardware. In the next two years ARRA stimulus funding will be used to upgrade many data loggers throughout the CISN, reducing latency by 3–5 s at these sites. The current statistical median latency is 5.2 s. With these upgrades we anticipate this will be reduced to 2–3 s.

We expect many improvements to the ElarmS code and the CISN networks during the coming three years. Learning from the realtime experience of the last three years, the ElarmS, VS, and Onsite methodologies will be integrated into a single prototype system. New code is being written to reduce processing delays and hardware upgrades will reduce data transmission latencies. The CISN is currently identifying a small group of about 10 test users who will soon start to receive alerts from the new prototype system, called the CISN ShakeAlert System.

References

- [1] Allen RM. Rapid magnitude determination for earthquake early warning. In: Manfredi G, editor. *The Many Facets of Seismic Risk*. Naples, Italy: University of Degli Studi di Napoli "Federico II"; 2004. p. 15–24.
- [2] Allen RM. Probabilistic warning times for earthquake ground shaking in the San Francisco Bay Area. *Seismol Res Lett* 2006;77(3):371–6.
- [3] Allen RM. The ElarmS earthquake early warning methodology and application across California. In: Gasparini P, editor. *Earthquake Early Warning*. Milan, Italy: Springer Ital.; 2007. p. 21–44.
- [4] Allen RM, Kanamori H. The potential for earthquake early warning in southern California. *Science* 2003;300:786–9.
- [5] Allen RM, Brown H, Hellweg M, Khainovski O, Lombard P, Neuhauser D. Real-time earthquake detection and hazard assessment by ElarmS across California. *Geophys Res Lett* 2009;36:L00B08.
- [6] Boatwright J, Bundock H, Luetgert J, Seekins L, Gee L, Lombard P. The dependence of PGA and PGV on distance and magnitude inferred from Northern California ShakeMap Data. *Bull Seismol Soc Am* 2003;93(5):2043–55.
- [7] Boore DM, Joyner WB, Fumal TE. Equations for estimating horizontal response spectra and peak accelerations from western North American earthquakes: a summary of recent work. *Seismol Res Lett* 1997;68(1):128–53.
- [8] Böse M, Hauksson E, Solanki K, Kanamori H, Heaton, TH. Real-time testing of the on-site warning algorithm in southern California and its performance during the July 29 2008 M_w 5.4 Chino Hills earthquake, L00B03. 2009.
- [9] Brown HM, Allen RM, Grasso VF. Testing ElarmS in Japan. *Seismol Res Lett* 2009;80(5):727–39.
- [10] Cua G, Fischer M, Heaton T, Wiemer S. Real-time performance of the Virtual Seismologist earthquake early warning algorithm in southern California. *Seismol Res Lett* 2009;80(5):740–7.
- [11] Hill DP, Eaton JP, Jones LM. Seismicity, 1980–86. In: Wallace RE, editor. *The San Andreas Fault System*, Vol. 1515. California: US Geol. Surv. Prof. Pap.; 1990. p. 115–52.
- [12] Iervolino I, Giorgio M, Galasso C, Manfredi G. Uncertainty in early warning predictions of engineering ground motion parameters: what really matters? *Geophys Res Lett* 2009;36:L00B06.
- [13] Lockman AB, Allen RM. Single-station earthquake characterization for early warning. *Bull Seismol Soc Am* 2005;95(6):2029–39.
- [14] Olson EL, Allen RM. The deterministic nature of earthquake rupture. *Nature* 2005;438(7065):212–5.
- [15] Tsang L, Allen RM, Wurman G. Magnitude scaling relations from P-waves in southern California. *Geophys Res Lett* 2007;34:L19304.
- [16] Wald DJ, Quitoriano V, Heaton TH, Kanamori H, Scrivner CW, Worden BC. TriNet ShakeMaps: rapid generation of instrumental ground motion and intensity maps for earthquakes in Southern California. *Earthquake Spectra* 1999;15(3):537–56.
- [17] Wald DJ, Worden BC, Quitoriano V, Pankow KL. *ShakeMap1 Manual: Technical manual, users guide, and software guide*, Tech. Methods 12–A1. Reston, VA: US Geol. Surv.; 2005.
- [18] Wurman G, Allen RM, Lombard P. Toward earthquake early warning in northern California. *J Geophys Res* 2007;112:B08311.
- [19] Youngs RR, Chiou S-J, Silva WJ, Humphrey JR. Strong ground-motion relationships for subduction zones. *Seism Res Lett* 1997;68(1):58–73.